Calibration of a SEIR–SEI epidemic model to describe the Zika virus outbreak in Brazil

Eber Dantas, Michel Tosin, Americo Cunha Jr*

Nucleus of Modeling and Experimentation with Computers – NUMERICO, Universidade do Estado do Rio de Janeiro – UERJ, Rua São Francisco Xavier, 524, Rio de Janeiro, RJ, 20550-900, Brasil

ARTICLE INFO

ABSTRACT

Multiple instances of Zika virus epidemic have been reported around the world in the last two decades, turning the related illness into an international concern. In this context the use of mathematical models for epidemics is of great importance, since they are useful tools to study the underlying outbreak numbers and allow one to test the effectiveness of different strategies used to combat the associated diseases. This work deals with the development and calibration of an epidemic model to describe the 2016 outbreak of Zika virus in Brazil. A system of 8 differential equations with 8 parameters is employed to model the evolution of the infection through two populations. Nominal values for the model parameters are estimated from the literature. An inverse problem is formulated and solved by comparing the system response to real data from the outbreak. The calibrated results presents realistic parameters and returns reasonable descriptions, with the curve shape similar to the outbreak evolution and peak value close to the highest number of infected people during 2016. Considerations about the lack of data for some initial conditions are also made through an analysis over the response behavior according to their change in value.

1. Introduction

The Zika virus is a flavivirus that upon infection in humans causes an illness, known as Zika fever, identified commonly with macular or papular rash, mild fever and arthritis [1,2]. It is mainly a vector-borne disease carried by the genus *Aedes* of mosquitoes [2,3], while in a lesser amount it is also transmitted via sexual interaction [4,5], and contamination by blood transfusion is under investigation [6]. The Zika virus was first isolated in primates from the Zika forest in Uganda in 1947 [7]. Evidences of the virus in humans were found in Nigeria in 1968 [8]. An epidemic occurred in 2007 on Micronesia [9], followed by multiple outbreaks on several Pacific Islands between 2013 and 2014 [10,11]. The first Zika virus autochthonous case in Brazil was reported around April, 2015 [12], and nearly 30, 000 cases of infection were already notified by January 30, 2016 [13], along with the Pan American Health Organization being informed in the same month about locally-transmitted cases on numerous continental and island territories of America [14]. The Brazilian Ministry of Health registered 215, 319 probable cases of Zika fever (130, 701 of which were confirmed) until the 52th epidemiological week (EW) of 2016 [12]. The Zika epidemic has been causing concern in the international medical community, health authorities and population, specially due to an association between the Zika virus and other diseases, such as newborn microcephaly [4,15] and Guillain-Barré

---

* Corresponding author.
   E-mail addresses: eber.paiva@uerj.br (E. Dantas), michel.tosin@uerj.br (M. Tosin), americo@ime.uerj.br (A. Cunha Jr).
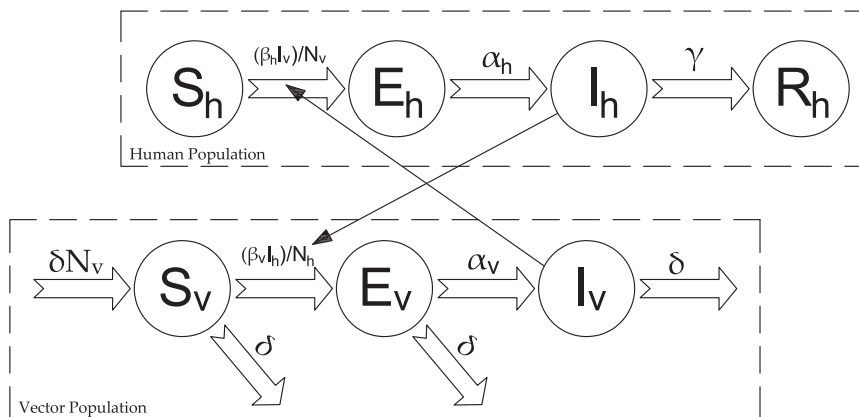
Fig. 1. Schematic representation of the SEIR–SEI model for the Zika virus outbreak description.

syndrome [16], whose correlation to the Zika virus was considered by the World Health Organization a *"scientific consensus"* [17].

In this epidemic scenario, the development of control and prevention strategies for the mass infection is a critical issue. A mathematical model capable of providing a description of the infected people throughout an outbreak is a useful tool that can be employed to identify effective and vulnerable aspects on disease control programs [18–20]. Furthermore, for an epidemic model to be truly useful it must undergo a judicious process of *validation* [21,22], which consists in comparing model predictions with real data in order to evaluate if they are realistic. In general, the first predictions of a model do not agree with the observations, possibly due to inadequacies in the model hypotheses or because of a poor choice for the model nominal parameters. The first case invalidates the model, but the second can be amended through a procedure known as *model calibration*, where a set of parameters that promote a good agreement between predictions and observations is sought.

This work is one of the results in a rigorous ongoing process of identification and validation of representative models to describe Zika virus outbreaks in Brazil [23,24]. For this purpose, a SEIR-SEI mathematical model is adapted to the Brazilian scenario. This specific SEIR-SEI description has been successfully used before for the outbreaks in Micronesia [25] and French Polynesia [26]. Some assumptions were also based on similar studies performed over SEIR dynamical systems [27–30]. The nominal values of the model parameters belong to characteristics of the Zika infection and its vector, quantitatively estimated in the literature or published by health organizations. Predictions are obtained from numerical simulation and further heuristic manipulation, followed by a comparison to real data of the outbreak as an initial effort to validate the model. In sequence, a rigorous process of model calibration is performed through the formulation and solution of an inverse problem.

The rest of this paper is organized as follows. In Section 2, the mathematical model is described and estimation of nominal values for the model parameters is discussed. In Section 3, the forward and inverse problems are formulated and solved, where results are detailed and a subsequent comparison between model predictions and experimental data is made to calibrate the model. Finally, in Section 4, the main contributions of this work are emphasized and a path for future works is suggested.

2. Epidemic model for Zika virus dynamics

2.1. Model hypotheses

This work utilizes a variant of the Ross–Macdonald model [31] for epidemic predictions, separating the populations into a SEIR–SEI framework (susceptible, exposed, infectious, recovered) [32–34]. Each category represents the health condition of an individual inside such group at time t, with respect to the considered infection. The susceptible group, denoted by $S(t)$, represents those who are uncontaminated and are able to become infected. The exposed portion of the population, $E(t)$, comprehends anyone that is carrying the pathogen but is still incapable of transmitting the disease. While the infectious individuals, $I(t)$, can spread the pathogen and may display symptoms associated with the illness. Finally, the recovered group, $R(t)$, contains those who are no longer infected. The populations of humans and vectors are segmented into the aforesaid classes (excepting the group of recovered vectors), as Fig. 1 depicts schematically with the accordingly subscripts. S_h, E_h, I_h and R_h amass the number of people at each stage of the model description, and S_v, E_v, I_v signifies proportion of vectors ($0 \leq S_v$, E_v, $I_v \leq 1$ and $S_v + E_v + I_v = 1$).

Demographic changes in the number of humans are not considered because the timescale of infection is much faster than the timescale of birth and deaths for the latter to significantly alter the development of the disease in the Brazilian context (supplementary material B provides tools to test this assertion). The total vector population is maintained constant

during the analysis, although variations of the proportion of vectors on the particular compartments are introduced via birth and death rates. The vector in question is regarded as a hypothetical mosquito apt to being infected or infectious throughout all its lifetime – which means the model accounts only for the adult stage of their life cycle – and also unable to recover.

The time elapsed while an individual is on the aforementioned exposed group is known as the latent period of an organism and, in this work, is adopted as equivalent to the commonly called incubation period (the time elapsed between being infected and exhibiting symptoms), since data is extremely sparse on the latter for humans [35] (namely, the intrinsic incubation period). Both terms are used interchangeably hereafter, and the concepts do not differ on the mosquitoes case (the extrinsic incubation period) [36]. In addition, all the members of the susceptible group are treated as equally capable of being infected and the recovered ones as completely immunized.

2.2. Model equations

The evolution of individuals through the SEIR–SEI groups is governed by the following (nonlinear) autonomous system of ordinary differential equations

$$
\begin{aligned}
\frac{dS_h}{dt} &= -\beta_h S_h \frac{I_v}{N_v}, & \frac{dS_v}{dt} &= \delta N_v - \beta_v S_v \frac{I_h}{N_h} - \delta S_v, \\[2mm]
\frac{dE_h}{dt} &= \beta_h S_h \frac{I_v}{N_v} - \alpha_h E_h, & \frac{dE_v}{dt} &= \beta_v S_v \frac{I_h}{N_h} - (\alpha_v + \delta) E_v, \\[2mm]
\frac{dI_h}{dt} &= \alpha_h E_h - \gamma I_h, & \frac{dI_v}{dt} &= \alpha_v E_v - \delta I_v, \\[2mm]
\frac{dR_h}{dt} &= \gamma I_h, & \frac{dC}{dt} &= \alpha_h E_h,
\end{aligned}
\tag{1}
$$

where N represents the total population and $1/\alpha$ the disease's incubation period (each with the corresponding subscript of h for human's and v for vector's), $1/\delta$ means the vector lifespan, $1/\gamma$ is the human infection period – which is defined in this work as the interval of time that a human is infectious — and β identifies the transmission rate, specifically β_h is the mosquito-to-human rate and β_v the human-to-mosquito rate.

The transmission terms $\beta_h S_h I_v/N_v$ and $\beta_v S_v I_h/N_h$ are composed by a number of susceptible individuals (S_h, S_v, respectively), a transmission rate (β_h, β_v) and the probability of the contact being made with an infectious member of the other population (I_v/N_v, I_h/N_h). Both transmissions terms come from the assumption that the rate of contacts is constant, which characterizes a frequency-dependent transmission [37].

The compartmentalization hypothesis requires setting the variables at the initial time of the analysis, t_0, such that their sum equals the total population in each case, e.g, $S_v(t_0) + E_v(t_0) + I_v(t_0) = N_v = 1$. By so doing, for all $t > t_0$, $S_h(t)$, $E_h(t)$, $I_h(t)$ and $R_h(t)$ will always add up to N_h; and $N_v(t)$ will be the equilibrium solution of the initial value problem

$$
\frac{dN_v}{dt} = \delta (1 - N_v(t)), \quad N_v(t_0) = 1,
\tag{2}
$$

namely, $N_v(t) = 1$. This consideration allows the simplification of treating the total vector population as a parameter N_v, instead of a variable, since it stays constant throughout the analysis. If one wishes to treat the vector population as a variable, a recruitment parameter would need to be added in place of δN_v as well as another differential equation to account for the changes in $N_v(t)$.

The dC/dt equation allows evaluation of the cumulative number $C(t)$ of infectious people until the time t, that is, the amount of humans so far that contracted the disease and have passed through or are in the infectious group at the given time.

Additionally, a set of $M = 52$ points to represent the number of new infectious cases of Zika fever at each week is defined as follows:

$$
\mathcal{N}_w = C_w - C_{w-1}, \quad \mathcal{N}_1 = C_1, \quad w = 2, \ldots, 52,
\tag{3}
$$

where C_w is the cumulative number of infectious humans in the w-th EW.

Fig. 2 organizes the data of cumulative number of infectious and new cases per week provided by the Brazilian Ministry of Health [38] (supplementary material A) for 2016, where the evolution of the infection can be seen. The expected behavior for the model is that it generates a seemingly year long outbreak for 2016 that matches $C(t)$ and $\mathcal{N}_w$ to the data of Fig. 2. The end of this outbreak is marked by the exposed and infectious portions of vectors reaching very low values, effectively killing off the contamination process to the point that $S_h(t)$ stabilizes.

2.3. Nominal parameters

The preliminary values for the parameters of the set of Eqs. (1) come from the related literature concerning the Zika infection, vector-borne epidemic models, the *Aedes aegypti* mosquito (which is the main vector for Zika, Dengue and
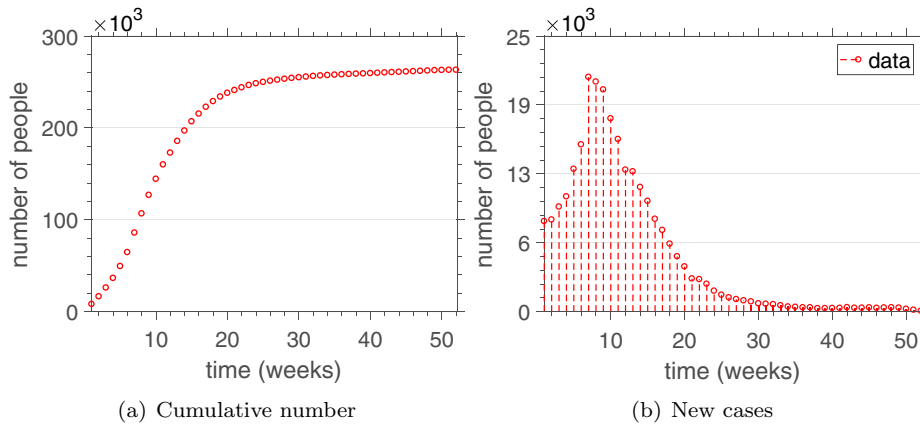
Fig. 2. Outbreak data.

Yellow fever in Brazil) and publications provided by health organizations and government agencies. The Brazilian Institute of Geography and Statistics reports that Brazil had approximately $N_h = 206 \times 10^6$ people by July, 2016 [39], and N_v is set 1 to entail an entire vector population. The adopted extrinsic incubation period is $1/\alpha_v = 9.1$ days [25]. This value agrees with other statistical confidence intervals (CI) that are presented for the parameter in another works (95% CI: 7.3–9.3 days [40]) and is close to the numbers suggested by experimental studies for the time necessary for the virus to reach the mosquito's saliva after an infectious blood meal (5 [41,42] and 7 days [43]). A systematic review and pooled analysis of the literature and case studies available in [44] estimates that the median intrinsic incubation period is 5.9 days (95% CI: 4.4–7.6). This values is selected for $1/\alpha_h$ in this work and is compatible with the range of 3–12 days recommended by multiple sources [15,45,46], also formerly used in previous studies [47]. The aforementioned literature analysis in [44] also concludes that 9.9 (95% CI: 6.9-21.4) days is the mean time until an infected has no detectable virus in blood. Considering the assumption that the infectiousness in Zika infection ends 1.5-2 days before the virus becomes undetectable [25,40], the chosen value for the human infectious period is $1/\gamma = 9.9 - 2 = 7.9$ days. As for the vector lifespan $1/\delta$, "*the adult stage of the mosquito is considered to last an average of eleven days in the urban environment*" according to Otero et al. [48]. This is the assumed value for the parameter in this work, which is also consistent with the usual life expectancy for the mosquito in Rio de Janeiro, Brazil [49], and comes close to the average of 2–3 weeks considered in biological studies about the species [50] and by the Centers for Disease Control and Prevention [51]. Lastly, the time between a mosquito being infected and it infecting a human, $1/\beta_h$, and the time between a human infection and a mosquito taking an infectious blood meal, $1/\beta_v$, is estimated in [40] as an average of 11.3 days (95% CI: 8.0–16.3) and 8.6 days (95% CI: 6.2–11.6), respectively.

3. Calibration of the epidemic model

3.1. Forward problem

The epidemic model of Section 2, supplemented by an appropriate set of initial conditions, is a continuous-time dynamical system

$$\dot{\mathbf{x}}(t) = \mathbf{f}(\mathbf{x}(t), \mathbf{p}), \quad \mathbf{x}(t_0) = \mathbf{x}_0 \tag{4}$$

where $\mathbf{x}(t) = (S_h(t), E_h(t), I_h(t), R_h(t), S_v(t), E_v(t), I_v(t), C(t)) \in \mathbb{R}^8$ is the vector of states at time t, $\mathbf{x}_0 = \left(S_h^i, E_h^i, I_h^i, R_h^i, S_v^i, E_v^i, I_v^i, C^i\right) \in \mathbb{R}^8$ is a prescribed initial condition vector referring to the initial time t_0 of the analysis, the vector $\mathbf{p} = (N_h, \beta_h, \alpha_h, \gamma, N_v, \beta_v, \alpha_v, \delta) \in \mathbb{R}^8$ lumps the model parameters and $\mathbf{f} : U \subset \mathbb{R}^8 \times \mathbb{R}^8 \to \mathbb{R}^8$ is a nonlinear map which gives the evolution law of this dynamics, defined (for fixed t) on the open set

$$U = \left\{ (\mathbf{x}(t), \mathbf{p}) \in \mathbb{R}^8 \times \mathbb{R}^8 \mid x_n(t) > 0 \text{ and } p_n > 0, \text{ for } n = 1, \ldots, 8 \right\}. \tag{5}$$

The forward problem consists in providing initial conditions (IC) and a set of parameters, represented by the pair $\boldsymbol{\alpha} = (\mathbf{x}_0, \mathbf{p})$, and compute by means of numerical integration the model response $\mathbf{x}(t)$ from which a scalar observable $\boldsymbol{\phi}(\boldsymbol{\alpha}, t)$ is obtained. In the forward problem, $\boldsymbol{\alpha}$ represents all IC and system parameters from Eq. (1), while $\boldsymbol{\phi}(\boldsymbol{\alpha}, t)$ is the new cases $\mathcal{N}_w$ system response from Eq. (3).

Since the map $\mathbf{f}$ has a polynomial nature in $\mathbf{x}$, it is a continuously differentiable function in $\mathbf{x}$. Thus, the existence and uniqueness theorem for ordinary differential equations guarantees that the initial value problem of (4) has an unique solution. Besides that, one can also show that this solution is continuously dependent on $\boldsymbol{\alpha}$, as well as the *forward map* $\boldsymbol{\phi}$ [52,53].

The evaluation of the system response in the *forward problem* is performed numerically in this work via a Runge–Kutta (4,5) method and the scalar observable of interest $\mathcal{N}_w$ is used to assess the simulation when compared with real data of

(a) Cumulative number   (b) New cases
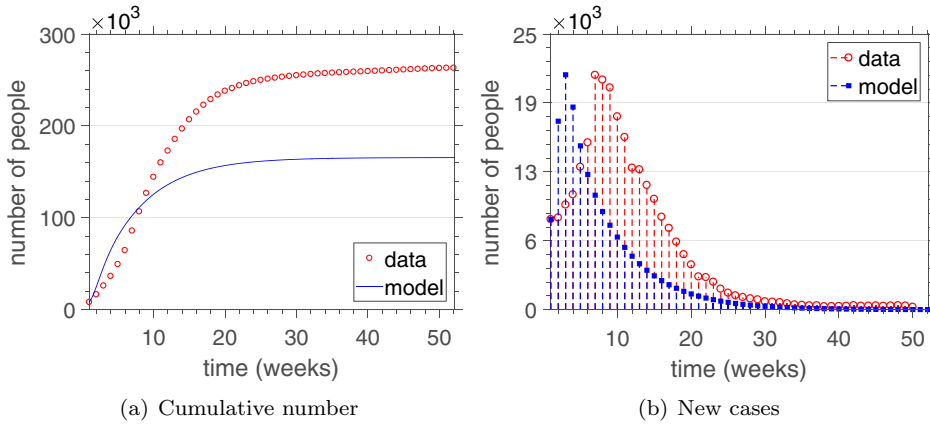
Fig. 3. Outbreak data (red) and model response using the nominal parameters (blue). (For interpretation of the references to color in this figure legend, the reader is referred to the web version of this article.)

the 2016 outbreak made available by the Brazilian Ministry of Health [38] (supplementary material A). The referred data consists of probable cases of infected people per EW, registered by sanitary outposts and health institutions throughout the country when the common symptoms of Zika fever were exhibited by an individual. In accordance with the hypothesis that one only displays symptoms when inside $I_h(t)$, the $C(t)$ variable models this discrete accumulating data on a continuous sense and $\mathcal{N}_w$ provides the corresponding influx per EW. The $C(t)$ time series is also observed as a criteria for good fitting, since it signifies the general impact of the epidemic and because a reasonable $\mathcal{N}_w$ result does not necessarily implies an acceptable cumulative number of infectious individuals for all t in comparison to the data.

The initial time of the analysis was established as the first EW of 2016. The remaining individuals in both populations are assumed susceptible at first, meaning $S_h^i = N_h - E_h^i - I_h^i - R_h^i$ and $S_v^i = N_v - E_v^i - I_v^i$. The initial values for the exposed and infectious groups are set equal, $E_h^i = I_h^i$ and $E_v^i = I_v^i$. Likewise, the number of infected humans at the initial time must be $I_h^i = C^i$, given its definition. The value of C^i is taken as the number of confirmed Zika cases in Brazil on the first EW of 2016 [38], 8, 201 individuals, and the recovered group is assumed equal to the suspected number of infected in 2015, according to the data available [13], $R_h^i = 29{,}639$ individuals. As for the proportion of infectious vectors in the first week, to work around the lack of data for this initial condition, repetitive manual estimations were tried until the resulted time series of $\mathcal{N}_w$ presented reasonable values compared to the real data. It became clear that the system response is very sensible to I_v^i, as slight variations in its value are required to achieve feasible results. In the process of choosing its value, the matching of the $\mathcal{N}_w$ curve's peak to the amplitude of infection is also a priority, since this is the main interest region for evaluation of the outbreak. The nominal values of the parameters exhibited viable $\mathcal{N}_w$ curves around $I_v^i = 2.2 \times 10^{-4}$.

Fig. 3 presents the SEIR–SEI model response for the nominal set of parameters from Section 2.3, supplied with the above IC, on an epidemiological week temporal domain consisting of one to fifty-two weeks (7 to 365 days), compared with the data of the outbreak (red dots).

The general shape of the curves in Fig. 3 do provide qualitative information regarding the evolution of the infection, even though the portrayed descriptions are not quantitatively realistic. This inherent pattern agreement and numerical mismatch suggests that the model response may differ from the real data due to the use of unsuitable values for the parameters or incorrect IC assumptions. The search for parameter and initial condition values that make the simulations fit well to the observed data defines model calibration (or system identification), being the object of interest of the next section.

3.2. Inverse problem

The model calibration problem seeks to find a set of parameters that, to a certain degree, makes the model response as close as possible to the empirical observations (reference data), once, due to the erros on model conception and reference data acquisition, it is (practically) impossible for the forward map to reproduce the outbreak observations.

The mathematical setting for this case considers the *parameters vector* $\boldsymbol{\alpha}$ defined in the *parameter space* $E = \mathbb{R}^{12}$, since here $\boldsymbol{\alpha}$ comprises all IC and system parameters from Eq. (1), excepting N_h, N_v, R_h^i and C^i, which are kept fixed in their nominal values. For the purpose of comparison between observations and predictions, a discrete set with M time-instants is considered, so that scalar observations and predictions are respectively lumped into $\boldsymbol{y} = (y_1, y_2, \ldots, y_M)$ and $\boldsymbol{\phi}(\boldsymbol{\alpha}) = (\phi_1, \phi_2, \ldots, \phi_M)$, both defined in the *data space* $F = \mathbb{R}^M$. Note that the *forward map* $\boldsymbol{\phi} \colon E \to F$ associates to each parameters vector $\boldsymbol{\alpha}$ an observable vector $\boldsymbol{\phi}(\boldsymbol{\alpha})$ where the component represents the number of new cases in each week of the year, i.e., $\phi_w = \mathcal{N}_w$. In practice, the parameters vector is restricted to be on the convex *set of admissible values* $C = \{\boldsymbol{\alpha} \in E \mid \mathbf{lb} \le \boldsymbol{\alpha} \le \mathbf{ub}\}$, in which **lb** and **ub** are lower and upper vector bounds for $\boldsymbol{\alpha}$, respectively.
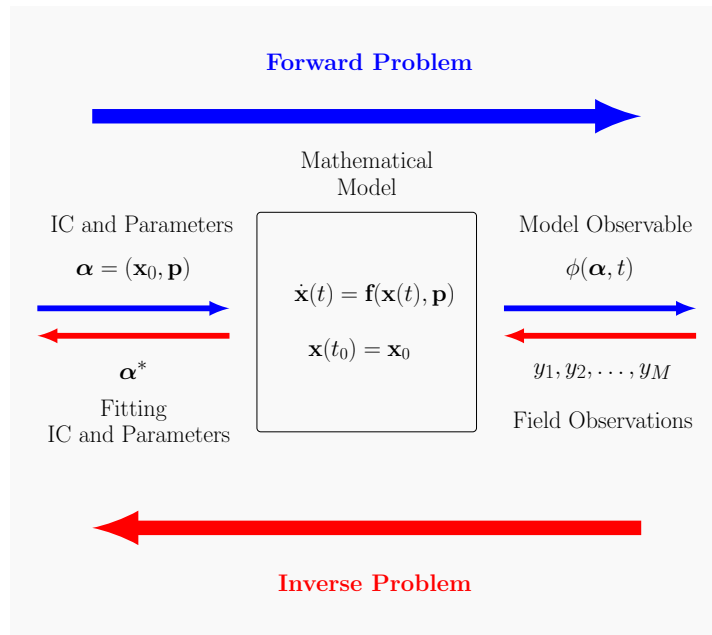
Fig. 4. Schematic representation of the forward and inverse problems associated to the epidemic model.

In formal terms, given an *observation vector* $\mathbf{y} \in F$ and a *prediction vector* $\boldsymbol{\phi}(\boldsymbol{\alpha}) \in F$, the calibration aims at finding a vector of parameters $\boldsymbol{\alpha}^*$ such that

$$\boldsymbol{\alpha}^* = \arg\min_{\boldsymbol{\alpha} \in C} J(\boldsymbol{\alpha}) , \tag{6}$$

for a misfit function

$$J(\boldsymbol{\alpha}) = ||\mathbf{y} - \boldsymbol{\phi}(\boldsymbol{\alpha})||^2 = \left\{ \sum_{m=1}^{M} \left| y_m - \phi_m(\boldsymbol{\alpha}) \right|^2 \right\}. \tag{7}$$

This is the *inverse problem* associated to the epidemic model. In general this type of problem is extremely nonlinear, with none or low regularity, multiple solutions (or even none), being much more complicated to attack in comparison with the forward problem [54,55]. A schematic representation of the forward and the inverse problem associated to the epidemic model is shown in Fig. 4.

This inverse problem attempts to estimate a finite number of parameters on a finite dimension space, being defined in terms of a typical nonlinear misfit function. Therefore, Theorem 4.5.1 of Chavent [56] can be invoked to guarantee a proper sense of well-posedness (existence, unimodality and local stability) for the inverse problem.

The Trust–Region–Reflective method (TRR) is employed here to numerically approximate a solution for the inverse problem (6). The main idea of the method is to minimize a simpler function that reflects the behavior of $J(\boldsymbol{\alpha})$ in a neighborhood (trust-region) around $\boldsymbol{\alpha}$. The simpler function is defined as dependent on the trial step $\mathbf{s}$, characterizing the Trust–Region subproblem, and its computation is optimized by restricting the subproblem to a two-dimensional subspace. The subspace is linear spanned by a multiple of the gradient $\mathbf{g}$ and (in the bounded case) a vector obtained in a scaled modified Newton step, used for the convergence condition $D(\boldsymbol{\alpha})^{-2}\mathbf{g}(\boldsymbol{\alpha}) = 0$, where D is a diagonal matrix that depends on $\boldsymbol{\alpha}$, $\mathbf{g}$, $\mathbf{lb}$, and $\mathbf{ub}$ [57]. Finally, the trial step is found through the subproblem as

$$\mathbf{s}^* = \arg\min_{\mathbf{s}} \left\{ \frac{1}{2}\mathbf{s}^{\mathrm{T}}Q\mathbf{s} + \mathbf{g}^{\mathrm{T}}\mathbf{s} \ | \ ||D\mathbf{s}||_2 \leq \Delta \right\}, \tag{8}$$

where Δ is a scalar associated with the trust region size; Q is a matrix involving D, a Jacobian matrix (also dependent on $\boldsymbol{\alpha}$, $\mathbf{g}$, $\mathbf{lb}$, and $\mathbf{ub}$) and an approximation of the Hessian matrix [57]. The quadratic approximation in Eq. (8) has well-behaved solutions [58] and if $J(\boldsymbol{\alpha} + \mathbf{s}) < J(\boldsymbol{\alpha})$ then $\boldsymbol{\alpha}$ is updated to $\boldsymbol{\alpha} + \mathbf{s}$ and the process iterates, otherwise Δ is decreased. In addition, a reflection step also occurs if a given step intersects a bound: the reflected step is equivalent to the original step except in the intersecting dimension, where it assumes the opposite value after reflection.

The TRR algorithm also requires an initial guess for each parameter, identified in the next section as "TRR input". The stopping criteria are the norm of the step and the change in the value of the objective function, with a tolerance of 10^{-7}. Supplementary material B provides details on the software used for implementation.

(a) Cumulative number   (b) New cases
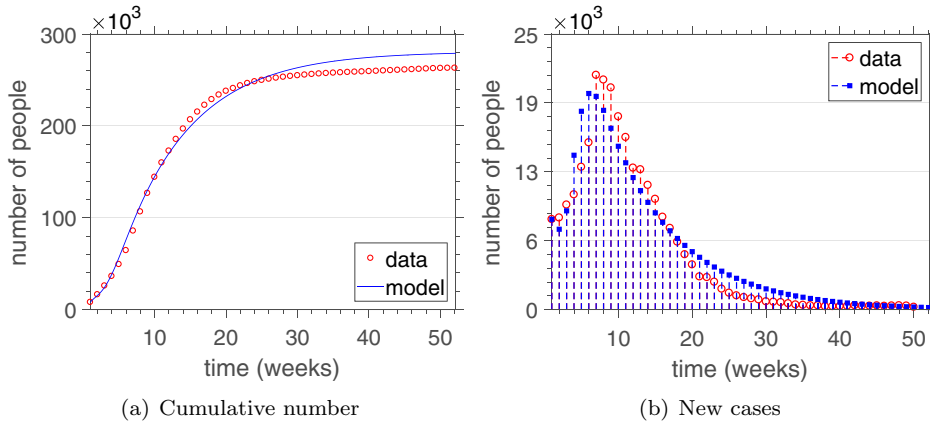
Fig. 5. Outbreak data (red) and calibrated model response (blue) from Table 1. (For interpretation of the references to color in this figure legend, the reader is referred to the web version of this article.)

Table 1

TRR setup for Fig. 5 calibrated response. The values referring to parameters are in days^{-1}, human IC are expressed in individuals, and vector quantities in proportion.

α	TRR input	lb	ub	TRR output	Reference
α_h	1/5.9	1/12	1/3	1/12	[15,40,44–47]
α_v	1/9.1	1/10	1/5	1/10	[40,41,43]
γ	1/7.9	1/8.8	1/3	1/8.8	[25,40,47]
δ	1/11	1/21	1/11	1/16.86	[47,49–51]
β_h	1/11.3	1/16.3	1/8	1/16.3	[40]
β_v	1/8.6	1/11.6	1/6.2	1/11.6	[40]
S_h^i	205, 953, 959	$0.9 \times N_h$	N_h	205, 700, 000	————
E_h^i	8201	0	N_h	15, 089	————
I_h^i	8201	0	N_h	253, 360	————
S_v^i	0.99956	0.99	0.999	1	————
E_v^i	2.2×10^{-4}	0	1	0	————
I_v^i	2.2×10^{-4}	0	1	0	————

3.3. Numerical experiments for calibration

Fig. 5 presents the best result for the $\mathcal{N}_w$ system response fitting problem using the nominal parameters and IC from Sections 2.3 and 3.1 as initial guesses for the TRR algorithm. The upper and lower bounds used for the parameters were set compatible with the literature suggested intervals and are presented in Table 1, along with the parameters and IC values resulted from the calibration ("TRR output"). The **ub** for δ was assumed lower than the **lb** for α_v to maintain consistency with the model interpretation. The minima for S_h^i and S_v^i were set to $0.9 N_h$ and 0.99, respectively, to establish a high number of susceptible individuals as is expected for the beginning of an outbreak. Also, the lower and upper bound (0.999) for S_v^i were motivated by noticing how variations in E_v^i and I_v^i of order 10^{-3} already bring significant changes in the system response. The lack of available data for the exposed and infectious groups at the onset of the epidemic was circumvented by appointing its minimum and maximum possible values as **lb** and **ub**, i.e., E_v^i and I_v^i were restricted between zero and one, while E_h^i and I_h^i were bounded by zero and N_h.

Additionally, to ensure the model hypotheses of compartmentalization and constant population, two additional fitting points were defined, $\Sigma_h = S_h^i + E_h^i + I_h^i$ and $\Sigma_v = S_v^i + E_v^i + I_v^i$, which were set to match $N_h - R_h^i$ and $N_v = 1$ on Eq. (6), respectively. However, the algorithm is only capable of approximating Σ_h and Σ_v to their intended values. So to account for these minor differences, the resulting values of $(N_h - R_h^i) - \Sigma_h$ and $1 - \Sigma_v$ were added to the TRR output of S_h^i and S_v^i. These corrections did not impact the calibration, since the scale of the differences would always be, correspondingly, 10^{-4} and 10^{-2} (at most), which are below the sensibility of S_h^i and S_v^i; thus, they were only exacted to keep the hypotheses rigorously sustained, otherwise the sum of the compartments in each population would quickly tend to N_h and N_v in an asymptotic fashion.

Clearly, Fig. 5 is a reasonable description of the outbreak: the general shape of the infection evolution is attained, all parameters are within realistic possibilities, the $C(t)$ curve overshoots the data by merely 6.00%, the peak value of $\mathcal{N}_w$ differs from the empirical data maximum by 7.87% and is only one week off. However, taking into consideration the order of magnitude of the first data point ($C^i = 8,201$) and the scale of the infection (215, 319 probable cases until the 52th EW [12]), the TRR output for I_h^i (253, 360) is probably too high, even though there is no reference value to compare with the

(a) Cumulative number   (b) New cases
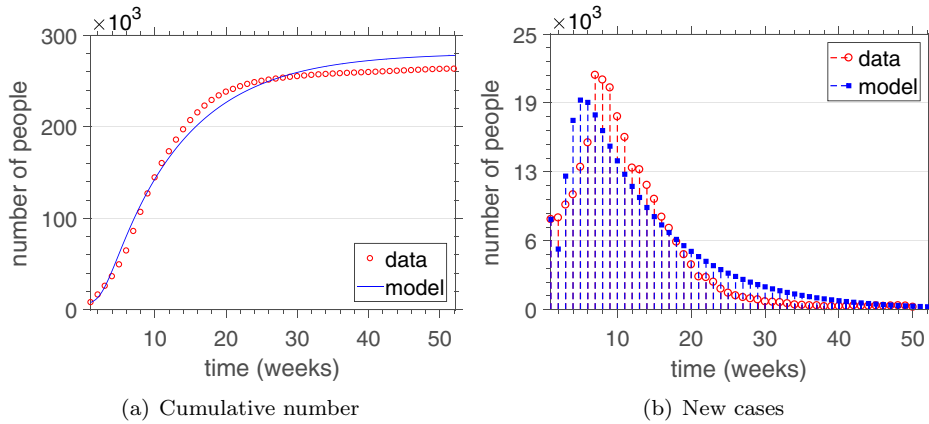
Fig. 6. Outbreak data (red) and calibrated model response (blue) from Table 2. (For interpretation of the references to color in this figure legend, the reader is referred to the web version of this article.)

Table 2
TRR setup for Fig. 6 calibrated response. The values referring to parameters are in days^{-1}, human IC are expressed in individuals, and vector quantities in proportion.

α	TRR input	lb	ub	TRR output	Reference
α_h	1/5.9	1/12	1/3	1/12	[15,40,44–47]
α_v	1/9.1	1/10	1/5	1/10	[40,41,43]
γ	1/7.9	1/8.8	1/3	1/3	[25,40,47]
δ	1/11	1/21	1/11	1/21	[47,49–51]
β_h	1/11.3	1/16.3	1/8	1/10.40	[40]
β_v	1/8.6	1/11.6	1/6.2	1/7.77	[40]
S_h^i	205,953,959	$0.9 \times N_h$	N_h	205,953,534	—————
E_h^i	8201	0	10,000	6827	—————
I_h^i	8201	0	10,000	10,000	—————
S_v^i	0.99956	0.99	0.999	0.999586	—————
E_v^i	2.2×10^{-4}	0	1	4.14×10^{-4}	—————
I_v^i	2.2×10^{-4}	0	1	0	—————

number of infectious individuals at the beginning of 2016, making it difficult to ascertain on a deterministic manner what is a feasible value for I_h^i.

Fig. 6 allows examination of the system behavior when the I_h^i value is around C^i, by depiction of another result to the inverse problem when the upper bound of the initial number of infectious individuals is set to 10,000. The same restriction was made over E_h^i merely to simplify the analysis. Table 2 displays the resulting parameters and IC.

The model response for a 10,000 I_h^i restriction also presents acceptable predictions of the general shape and numbers of the outbreak, even though it is less accurate than Fig. 5 on a fitting criteria for $\mathcal{N}_w$. For comparison, the $\mathcal{N}_w$ peak and data maximum difference increased to 10.57% and two weeks, while the overshoot on the $C(t)$ time series actually reduced to 5.74%.

To compare the two systems defined by the parameters and IC from each table, Fig. 7 portrays their I_h response. The system from Table 1 has an almost monotonically decreasing I_h curve, except for a slight local maximum around the 6th EW, while the system from Table 2 presents a significant increase in the number of infectious individuals by the same time, which correspond to the weeks right before the peak infection. As stated, the lack of empirical data for the current number of infectious at each EW makes it impossible to determine what is a quantitatively reasonable prediction for I_h values. But this work assumes that a more possible scenario involves a I_h time series that also follows the general shape of an epidemic curve around the weeks of maximum infection, especially considering that Fig. 7(a) implicates the notion that most people were infected strictly before 2016, which does not seems the case suggested by the Brazilian outbreak data of probable cases of infected per EW [12] when compared to numbers available for 2015 [13]. Thus, with this qualitative criteria in mind, the system from Table 2 is selected for a further analysis over its behavior dependency to the I_h^i initial condition.

Fig. 8 displays the $C(t)$, $\mathcal{N}_w$ and $I_h(t)$ responses per EW for various I_h^i on the system with parameters from Table 2. To simplify the analysis, E_h^i is considered equal to I_h^i in each case. The remaining IC are the same from the Table. The pattern
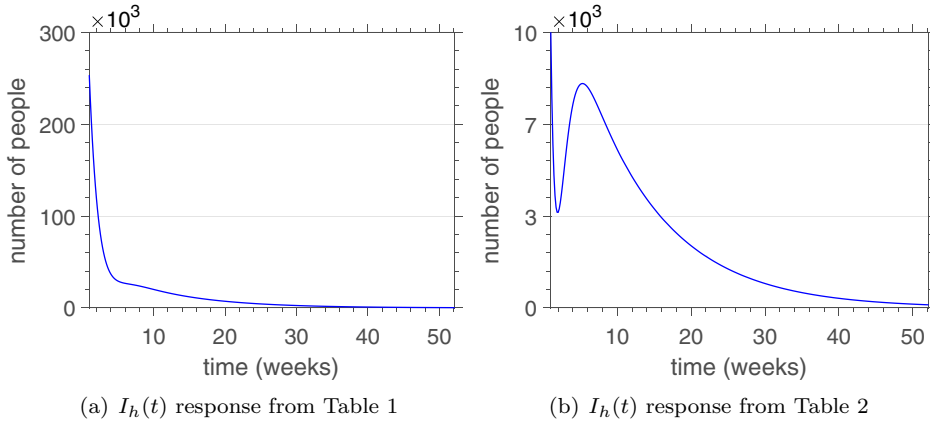
(a) $I_h(t)$ response from Table 1

(b) $I_h(t)$ response from Table 2

Fig. 7. Comparison between $I_h(t)$ responses from Table 1 (left) and Table 2 (rigth).

(a) Cumulative number

(b) New cases

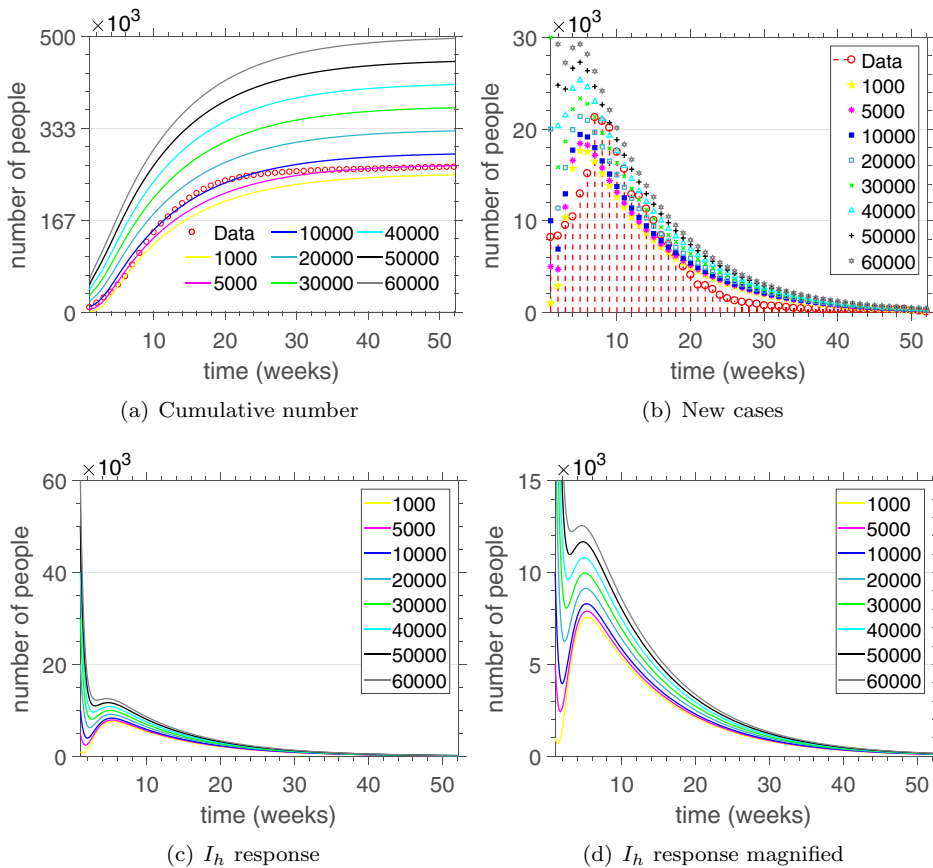(c) I_h response

(d) I_h response magnified

Fig. 8. Multiple $C(t)$, $\mathcal{N}_w$ and $I_h(t)$ responses per EW using the parameters from Table 2. The values on the legend correspond to the used I_h^i and E_h^i to generate the curves. The other IC are also from Table 2. The bottom right graph is the I_h comparison magnified around the local maximum region. The red circles are the previously used real data. (For interpretation of the references to color in this figure legend, the reader is referred to the web version of this article.)

suggests that a I_h^i increase on the system with this given set of parameters continuously escalates the $C(t)$ and $\mathcal{N}_w$ curves, eventually overshooting the data by far, and reduces the variations of $I_h(t)$ curve around its local maximum. Fig. 8 allows one to make better predictions about the outbreak by analyzing the multiple possible scenarios of epidemic evolution over different values for the IC missing empirical information. Clearly, the system response in all cases is qualitative reliable in simulating the outbreak ($C(t)$ and $\mathcal{N}_w$ shape) and can quantitatively approximate the real data values for some values of I_h^i.

4. Concluding remarks

A SEIR–SEI epidemic model to describe the dynamics of the 2016 Zika virus outbreak in Brazl is developed and calibrated in this work. Nominal quantities for the parameters are selected from the related literature concerning the Zika infection, the *Aedes aegypti* genus of mosquitoes, vector-born epidemic models and information provided by health organizations. The calibration process is done through the solution of an inverse problem with the aid of a Trust–Region–Reflective method, used to pick the best parameter values that would fit the model response for the number of new infectious cases per week into the disease's empirical data. Results within realistic values for the parameters are presented, stating reasonable descriptions with the curve shape similar to the outbreak evolution and proximity between the estimated peak value and data for maximum number of infected during 2016. Further analysis of the results about the lack of data for an initial condition is performed, exhibiting a range of values over which the system response keeps its quantitative reliability to a certain degree.

This work is part of a long project of modeling and prediction of epidemics related to the Zika virus in the Brazilian context [23,24]. In upcoming studies the authors intend to take into account the uncertainties underlying the model parameters via Bayesian updating and employ an Active Subspace approach [59–61] to explore relevant scenarios in parametric studies.

Supplementary material

Supplementary material associated with this article can be found, in the online version, at doi:10.1016/j.amc.2018.06.024.

References

[1] P. Brasil, Zika virus outbreak in Rio de Janeiro, Brasil: clinical characterization, epidemiological and virological aspects, PLoS Negl. Trop. Dis. 10 (4) (2016), doi:10.1371/journal.pntd.0004636.
[2] World Health Organization, Zika virus. www.who.int/mediacentre/factsheets/zika/en/, World Health Organization, 2016. Accessed: 08/18/2017.
[3] R.S. Fernandes, et al., Culex quinquefasciatus from Rio de Janeiro is not competent to transmit the local Zika virus, PLoS Negl. Trop. Dis. 10 (9) (2016), doi:10.1371/journal.pntd.0004993.
[4] E.E. Petersen, et al., Update: Interim Guidance for Preconception Counseling and Prevention of Sexual Transmission of Zika Virus for Persons with Possible Zika Virus Exposure– United States, 2016, MMWR Morb. Mortal. Wkly. Rep. 65 (39) (2016) 1077–1081, doi:10.15585/mmwr.mm6539e1.
[5] F.C. Coelho, et al., Higher incidence of Zika in adult women than adult men in Rio de Janeiro suggests a significant contribution of sexual transmission from men to women, Int. J. Infect. Dis. 51 (2016) 128–132, doi:10.1016/j.ijid.2016.08.023.
[6] I.J.F. Motta, B.R. Spencer, et al., Evidence for Transmission of Zika Virus by Platelet Transfusion, N. Engl. J. Med. 375 (11) (2016) 1101–1103, doi:10.1056/NEJMc1607262.
[7] G.W.A. Dick, S.F. Kitchen, A.J. Haddow, Zika virus (I). Isolations and serological specificity, Trans. R. Soc. Trop. Med. Hyg. 46 (5) (1952) 509–520, doi:10.1016/0035-9203(52)90042-4.
[8] D.L. Moore, et al., Arthropod-borne viral infections of man in Nigeria, Ann. Trop. Med. Parasitol 69 (1) (1975) 49–64, doi:10.1080/00034983.1975.11686983. 1964–1970
[9] M.R. Duffy, et al., Zika virus outbreak on Yap Island, Federated States of Micronesia, N. Engl. J. Med. 360 (24) (2009) 2536–2543, doi:10.1056/NEJMoa0805715.
[10] V.M. Cao-Lormeau, et al., Zika virus, French Polynesia, South Pacific, 2013, Emerg. Infect. Dis 20 (6) (2014) 1085–1086, doi:10.3201/eid2006.140138.
[11] J. Tognarelli, et al., A report on the outbreak of Zika virus on Easter Island, South Pacific, 2014, Arch. Virol. 161 (3) (2016) 665–668, doi:10.1007/s00705-015-2695-5.
[12] Secretaria de Vigilância em Saúde, Boletim Epidemiolólico. Monitoramento Dos Casos de Dengue. Febre de chikungunya e febre pelo vírus Zika até a Semana Epidemiológica 52, Secretaria de Vigilância em Saúde, vol. 48(2017). http://portalarquivos.saude.gov.br/images/pdf/2017/abril/06/2017-002-Monitoramento-dos-casos-de-dengue–febre-de-chikungunya-e-febre-pelo-v–rus-Zika-ate-a-Semana-Epidemiologica-52–2016.pdf, Accessed: 08/18/2017.
[13] N.R. Faria, R.S.S. Azevedo, et al., Zika virus in the Americas: early epidemiological and genetic findings, Science 352 (6283) (2016) 345–349, doi:10.1126/science.aaf5036.
[14] M. Hennessey, M. Fischer, J.E. Staples, Zika virus spreads to new areas — Region of the Americas, MMWR Morb. Mortal. Wkly. Rep. 65 (3) (2016) 55–58, doi:10.15585/mmwr.mm6503e1. May 2015-January 2016.
[15] G. Valentine, L. Marquez, M. Pammi, Zika virus-associated microcephaly and eye lesions in the newborn, J. Pediatric. Infect. Dis. Soc. 5 (3) (2016) 323–328, doi:10.1093/jpids/piw037.
[16] T. dos Santos, et al., Zika virus and the Guillain-Barré syndrome – Case series from seven countries, N. Engl. J. Med. 375 (16) (2016) 1598–1601, doi:10.1056/NEJMc1609015.
[17] World Health Organization. Zika virus, Microcephaly and Guillain-Barré Syndrome – Situation Report, World Health Organization, 2016. http://www.who.int/emergencies/zika-virus/situation-report/7-april-2016/en/, Accessed: 08/18/2017.
[18] A. Naheed, D. Lucy, M. Singh, Numerical study of SARS epidemic model with the inclusion of diffusion in the system, Appl. Math. Comput. 229 (2014) 480–498, doi:10.1016/j.amc.2013.12.062.
[19] A. Huppert, G. Katriel, Mathematical modelling and prediction in infectious disease epidemiology, Clin. Microbiol. Infect. 19 (2013) 999–1005, doi:10.1111/1469-0691.12308.
[20] D.P. Lizarralde-Bejarano, S. Arboleda-Sánchez, M.E. Puerta-Yepes, Understanding epidemics from mathematical models: details of the 2010 dengue epidemic in Bello (Antioquia, Colombia), Appl. Math. Model. 43 (2017) 566–578, doi:10.1016/j.apm.2016.11.022.
[21] W.L. Oberkampf, C.J. Roy, Verification and Validation in Scientific Computing, Cambridge University Press, 2010. ISBN 978-0-521-11360-1.

[22] A. Cunha Jr, S. Ekwaro-Osire, A.C. Gonçalves, F.M. Alemayehu, Modeling and quantification of physical systems, in: Uncertainties in a Probabilistic Framework, Springer International Publishing, New York, 2017, pp. 127–156. Probabilistic Prognostics and Health Management of Energy Systems doi: 10.1007/978-3-319-55852-3_8.
[23] E. Dantas, M. Tosin, J. Peterson, V. Lopes, A. Cunha Jr, A mathematical analysis about Zika virus outbreak in Rio de Janeiro, in: Proceedings of the Fourth Conference of Computational Interdisciplinary Science (CCIS 2016), São José dos Campos, Brazil, 2016.
[24] E. Dantas, M. Tosin, A. Cunha Jr, Zika virus in Brazil: calibration of an epidemic model for 2016 outbreak, in: Proceeding Series of the Brazilian Society of Applied and Computational Mathematics, v. 6, n. 1, 2018, doi:10.5540/03.2018.006.01.0460.
[25] S. Funk, et al., Comparative analysis of Dengue and Zika outbreaks reveals differences by setting and virus, PLoS Negl. Trop. Dis. 10 (12) (2016), doi:10.1371/journal.pntd.0005173.
[26] A.J. Kucharski, S. Funk, R.M. Eggo, H.P. Mallet, W.J. Edmunds, E.J. Nilles, Transmission dynamics of Zika virus in island populations: a modelling analysis of the 2013–14 French Polynesia outbreak, PLoS Negl. Trop. Dis. 10 (5) (2016), doi:10.1371/journal.pntd.0004726.
[27] X. Wang, L. Wei, J. Zhang, Dynamical analysis and perturbation solution of an SEIR epidemic model, Appl. Math. Comput. 232 (2014) 479–486, doi:10.1016/j.amc.2014.01.090.
[28] Y. Wanga, J. Cao, A. Alsaedi, B. Ahmade, Edge-based SEIR dynamics with or without infectious force in latent period on random networks, Commun. Nonlinear Sci. Numer. Simul. 45 (2017) 35–54, doi:10.1016/j.cnsns.2016.09.014.
[29] M.A. Safi, A.B. Gumel, E.H. Elbasha, Qualitative analysis of an age-structured SEIR epidemic model with treatment, Appl. Math. Comput. 219 (22) (2013) 10627–10642, doi:10.1016/j.amc.2013.03.126.
[30] Y. Cai, Y. Kang, W. Wang, A stochastic SIRS epidemic model with nonlinear incidence rate, Appl. Math. Comput. 305 (2017) 221–240, doi:10.1016/j.amc.2017.02.003.
[31] D.L. Smith, K.E. Battle, S.I. Hay, C.M. Barker, T.W. Scott, F.E. McKenzie, et al., Ross, MacDonald, and a theory for the dynamics and control of mosquito – transmitted pathogens, PLoS Pathog. 8 (4) (2012), doi:10.1371/journal.ppat.1002588.
[32] F. Brauer, C. Castillo-Chavez, Mathematical Models in Population Biology and Epidemiology, second ed., Springer, 2012, doi:10.1007/978-1-4614-1686-9.
[33] F. Brauer, P. van den Driessche, J. Wu, Mathematical Epidemiology, Springer, 2008, doi:10.1007/978-3-540-78911-6.
[34] M. Martcheva, An Introduction to Mathematical Epidemiology, Springer, 2015, doi:10.1007/978-1-4899-7612-3_1. first ed.
[35] M. Chan, M.A. Johansson, The incubation periods of Dengue viruses, PLoS ONE 7 (11) (2012), doi:10.1371/journal.pone.0050972.
[36] J. Lessler, L.H. Chaisson, et al., Assessing the global threat from Zika virus, Science 353 (6300) (2016), doi:10.1126/science.aaf8160.
[37] M. Begon, M. Bennett, R.G. Bowers, et al., A clarification of transmission terms in host-microparasite models: numbers, densities and areas, Epidemiol. Infect. 129 (2002), doi:10.1017/S0950268802007148.
[38] Ministério da Saúde, Obtenção de nũMero de casos Confirmados de Zika, Por Município e Semana Epidemiológica, Ministério da Saúde, 2017, http://www.consultaesic.cgu.gov.br/busca/dados/Lists/Pedido/Item/displayifs.aspx?List=0c839f31-47d7-4485-ab65-ab0cee9cf8fe&ID=537263&Web=88cc5f44-8cfe-4964-8ff4-376b5ebb3bef, Accessed: 08/18/2017.
[39] Fundação Instituto Brasileiro de Geografia e Estatística, Diário Oficial da União, N. 167- Seção1, Imprensa Nacional, Brasília, (2016) 47–65.
[40] N.M. Ferguson, et al., Countering the Zika epidemic in Latin America, Science 353 (6297) (2016) 353–354, doi:10.1126/science.aag0219.
[41] P.S.J. Wong, M.I. Li, C.S. Chong, L.C. Ng, C.H. Tan, Aedes (Stegomyia) albopictus (Skuse): a potential vector of Zika virus in Singapore, PLoS Negl. Trop. Dis. 7 (8) (2013), doi:10.1371/journal.pntd.0002348.
[42] M.I. Li, P.S.J. Wong, L.C. Ng, C.H. Tan, Oral Susceptibility of Singapore Aedes (Stegomyia) aegypti (Linnaeus) to Zika Virus, PLoS Negl. Trop. Dis. 6 (8) (2012), doi:10.1371/journal.pntd.0001792.
[43] T. Chouin-Carneiro, A. Vega-Rua, et al., Differential Susceptibilities of Aedes aegypti and Aedes albopictus from the Americas to Zika Virus, PLoS Negl. Trop. Dis. 10 (3) (2016), doi:10.1371/journal.pntd.0004543.
[44] C.T. Ott, J.T. Lessler, et al., Times to key events in Zika virus infection and implications for blood donation: a systematic review, Bull. World Health Organ. 94 (2016) 841–849, doi:10.2471/BLT.16.174540.
[45] S. Ioos, H.P. Mallet, I.L. Goffart, V. Gauthier, T. Cardoso, M. Herida, Current Zika virus epidemiology and recent epidemics, Med. Mal. Infect. 44 (2014) 302–307, doi:10.1016/j.medmal.2014.04.008.
[46] European Centre for Disease Prevention and Control, Rapid risk assessment: microcephaly in Brazil potentially linked to the Zika virus epidemic, European Centre for Disease Prevention and Control, 2015, https://ecdc.europa.eu/sites/portal/files/media/en/publications/Publications/zika-/microcephaly-Brazil-rapid-risk-assessment-Nov-2015.pdf, Accessed:08/18/2017.
[47] D.A.M. Villela, L.S. Bastos, et al., Zika in Rio de Janeiro: assessment of basic reproduction number and comparison with dengue outbreaks, Epidemiol. Infect. 145 (8) (2017) 1649–1657, doi:10.1017/S0950268817000358.
[48] M. Otero, H.G. Solari, N. Schweigmann, A stochastic population dynamics model for Aedes Aegypti: formulation and application to a city with temperate climate, Bull. Math. Biol. 68 (8) (2006) 1945–1974. doi: 10.1007/s11538-006-9067-y.
[49] R.L. de Oliveira, R.M. de Freitas, C.T. Codeço, Daily survival rates and dispersal of Aedes aegypti females in Rio de Janeiro, Brazil, Am. J. Trop. Med. Hyg. 76 (4) (2007) 659–665.
[50] M.J. Nelson., Aedes aegypti: biology and ecology, in: Pan American Health Organization, Washington, D.C., 1986.
[51] National Center for Emerging and Zoonotic Infectious Diseases, Dengue and the Aedes aegypti mosquito, National Center for Emerging and Zoonotic Infectious Diseases, 2012, https://www.cdc.gov/dengue/resources/30jan2012/aegyptifactsheet.pdf, Accessed: 08/18/2017).
[52] M.W. Hirsch, S. Smale, R.L. Devaney, Differential Equations, Dynamical Systems, and an Introduction to Chaos, third ed., Academic Press, 2013.
[53] L. Perko., Differential Equations and Dynamical Systems, third ed., Springer, 2006.
[54] R. Aster, B. Borchers, C. Thurber, Parameter Estimation and Inverse Problems, second ed., Elsevier, 2012. ISBN 978-0-128-10092-9.
[55] F. Yaman, V.G. Yakhno, R. Potthast, a survey on inverse problems for applied sciences, Math. Probl. Eng., 2013 (2013), doi:10.1155/2013/976837.
[56] G. Chavent., Nonlinear Least Squares for Inverse Problems: Theoretical Foundations and Step-by-Step Guide for Applications, Springer, 2010, doi:10.1007/978-90-481-2785-6.
[57] T.F. Coleman, Y. Li., An interior, trust region approach for nonlinear minimization subject to bounds, SIAM J. Optim. 6 (2) (1996) 418–445, doi:10.1137/0806023.
[58] A.R. Conn, N.I.M. Gould, P.L. Toint, Trust Region Methods, SIAM, 2000.
[59] P.G. Constantine., Active Subspaces: Emerging Ideas for Dimension Reduction in Parameter Studies, SIAM, 2015, doi:10.1137/1.9781611973860.
[60] P. Diaz, P. Constantine, K. Kalmbach, E. Jones, S. Pankavich, A modified SEIR model for the spread of Ebola in Western Africa and metrics for resource allocation, Appl. Math. Comput. 324 (2018) 141–155, doi:10.1137/130916138.
[61] P.G. Constantine, E. Dow, Q. Wang, Active subspace methods in theory and practice: applications to kriging surfaces, SIAM J. Sci. Comput. 36 (4) (2014) 1500–1524, doi:10.1137/130916138.